Eur. Phys. J. AP **11**, 21–27 (2000)

THE EUROPEAN PHYSICAL JOURNAL
APPLIED PHYSICS

Neural control and transient analysis of the LCL-type resonant converter

S. Zouggar[1,a], H. Nait Charif[2], and M. Azizi[1]

[1] University Mohammed 1er, École Supérieure de Technologie, Oujda Hay EL QODS, Complexe Universitaire, BP 473, 60000 Oujda, Morocco
[2] Computer & Electrical Engineering department, College of Engineering Michigan State University, USA

Received: 17 July 1999 / Revised: 25 January 2000 / Accepted: 7 April 2000

Abstract. This paper proposes a generalised inverse learning structure to control the LCL converter. A feedforward neural network is trained to act as an inverse model of the LCL converter then both are cascaded such that the composed system results in an identity mapping between desired response and the LCL output voltage. Using the large signal model, we analyse the transient output response of the controlled LCL converter in the case of large variation of the load. The simulation results show the efficiency of using neural networks to regulate the LCL converter.

PACS. 84.30.Jc Power electronics; power supply circuits – 84.35.i Neural networks

1 Introduction

Resonant converters are widely used in many industrial applications as supplies for CO_2 laser, X-rays tubes, and radars. This paper is concerned with the resonant converter type LCL that operates over the resonant frequency (Fig. 1) [1,2]. This converter presents the advantages of operating at no load, full load and short load [1,2]. Moreover, due to the third order resonance, the LCL has a high dynamic control characteristic.

The resonant converters of power electronics are variable structure systems. In fact they are linear piecewise systems whose global behaviour is strongly non-linear [3]. Many researches avoided the non-linearity problem by linearising the system around a steady point and then applying linear control techniques [4,5]. However, this approach can not be applied in the case of a large change in the load.

In the particular context of the LCL-type resonant converter, the aim of the control scheme is to maintain the output voltage V_s constant in spite of the large change of the load (R_s). This paper proposes to use the generalised inverse learning structure [5] to control the LCL converter based on the feedforward neural networks.

Using the large signal model [7] of the LCL converter developed in [4], the equilibrium points, characterised by the output voltage, the operation frequency and the load, were determined. To obtain an inverse neural model of the LCL resonant converter, the network is trained using the output voltage of the converter and the load as an input vector, and the converter input frequency as the target output. The obtained inverse system is then cascaded with the LCL converter such that the composed system results in an identity mapping between desired response and the LCL output voltage. Thus the network acts directly as a controller.

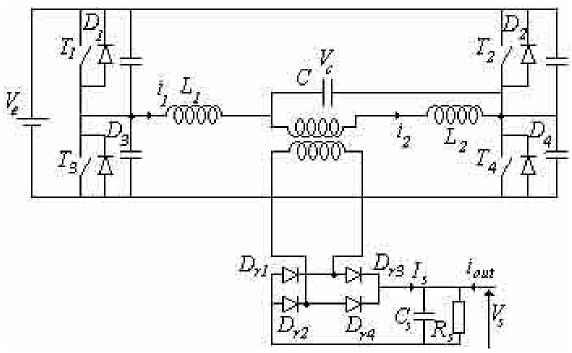

Fig. 1. Full bridge ZVS-LCL resonant converter.

Next section presents a brief description of the LCL converter and its operating mode. Section 3 gives the details of derivation of the discrete time domain model. Section 4 presents an overview of artificial neural network architecture and learning. The neural control scheme is presented in Section 5. The transient analysis of the output response is presented in Section 6.

2 Converter operation

Figure 1 presents the full-bridge ZVS-LCL resonant converter. Figure 2 illustrates the typical waveforms

[a] e-mail: zouggar@est.univ-oujda.ac.ma

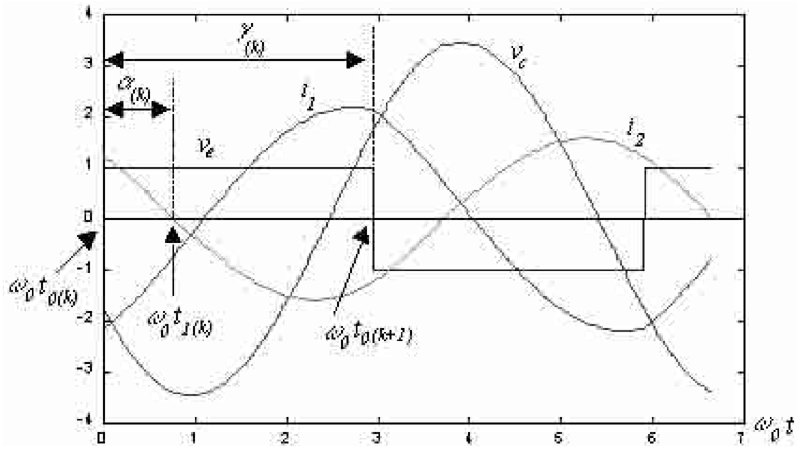

Fig. 2. Waves forms when $\frac{f}{f_0} = 1.04$.

starting from kth instant onwards, for the continuous current mode, in which the LCL converter operates.

In Figure 2, the diodes D_1 and D_4 are conducting at time instant $t_{0(k)}$. This being a lagging power factor mode of operation, the first inductor current i_1 has negative value at that instant, the second inductor current i_2 starts positive and becomes negative at the instant $t_{1(k)}$. At $t_{2(k)} \equiv t_{0(k+1)}$, T_1 and T_4 are turned off and the next half cycle begins with the conduction of D_2 and D_3.

The second half cycle is the same as the first half cycle except that all the variables have an opposite polarity. The first half cycle is called the kth event and the second half cycle is the $(k+1)$th event and so on. Each of these events is divided into sub-events depending upon the polarity of the second inductance current or the output voltage. The total conduction angle (switch and diode) is denoted by $\gamma_{(k)}$, as shown in Figure 2. The output voltage is controlled by varying the angle $\gamma_{(k)}$, where

$$\alpha_{(k)} = \omega_0 \left[t_{1(k)} - t_{0(k)}\right], \gamma_{(k)} = \omega_0[t_{0(k+1)} - t_{0(k)}],$$
$$\omega_0 = \frac{1}{\sqrt{L_0 C}} \text{ and } L_0 = \frac{L_1 L_2}{L_1 + L_2}\cdot$$

3 The discrete time domain model and the discrete state space model

3.1 The discrete time domain of the LCL converter

Under steady state conditions, the converter shows two possible operating modes, depending on the value of n, in each half cycle, where $\sigma = 1$ during mode 1 ($t_{0(k)} \leq t \leq t_{1(k)}$) and $\sigma = -1$ during mode 2 ($t_{1(k)} \leq t \leq t_{0(k+1)}$).

3.1.1 kth event

The equivalent circuit shown in Figure 3 is used in the analysis. The vector space equation for the LCL converter is:

$$[\dot{X}] = [A][X] + [B][U], \tag{1}$$

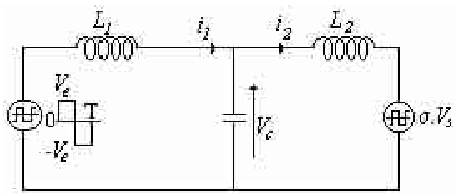

Fig. 3. The equivalent circuit.

where

$$[X] = \begin{bmatrix} \nu_\mathrm{c}^n \\ i_1^n \\ i_2^n \end{bmatrix}, [A] = \begin{bmatrix} 0 & 1 & -1 \\ -\frac{1}{\lambda} & 0 & 0 \\ \frac{1}{\beta} & 0 & 0 \end{bmatrix}, [B] = \begin{bmatrix} 0 & 0 \\ \frac{1}{\lambda} & 0 \\ 0 & \frac{-\sigma}{\beta} \end{bmatrix},$$
$$[U] = \begin{bmatrix} V_\mathrm{e}^n \\ V_\mathrm{s}^n \end{bmatrix}, K = L_1/L_2, \gamma = 1 + K, \beta = 1 + 1/K.$$

Using the normalised variables (*i.e.* per unit values), the general solutions of (1) in the time interval $t_{p-1} \leq t \leq t_p$ are:

$$\nu_\mathrm{c}^n(t) = \frac{V_\mathrm{e}^n}{\lambda} + \sigma\frac{V_\mathrm{s}^n}{\beta} + \left[\nu_\mathrm{c}^n(t_{p-1}) - \frac{V_\mathrm{e}^n}{\lambda} - \sigma\frac{V_\mathrm{s}^n}{\beta}\right]$$
$$\times \cos(\theta-\theta_{p-1}) + [i_1^n(t_{p-1}) - i_2^n(t_{p-1})]\sin(\theta-\theta_{p-1}) \tag{2}$$

$$i_1^n(t) - i_2^n(t) = -\left[\nu_\mathrm{c}^n(t_{p-1}) - \frac{V_\mathrm{e}^n}{\lambda} - \sigma\frac{V_\mathrm{s}^n}{\beta}\right]$$
$$\times \sin(\theta - \theta_{p-1}) + [i_1^n(t_{p-1}) - i_2^n(t_{p-1})]\cos(\theta - \theta_{p-1}) \tag{3}$$

where $V_\mathrm{b} = E, V_\mathrm{e}^n = \frac{E}{V_\mathrm{b}}, \nu_\mathrm{c}^n = \frac{\nu_\mathrm{c}}{V_\mathrm{b}}, i_1^n = i_1 \cdot \frac{Z}{V_\mathrm{b}},$

$$i_2^n = i_2 \cdot \frac{Z}{V_\mathrm{b}}, \omega^n = \frac{\omega}{\omega_0} \text{ and } Z = \sqrt{\frac{L_0}{C}}\cdot$$

In all the above equations $p = 1$ in mode 1 and $p = 2$ in mode 2.

3.1.2 $(k+1)$th event

The $(k+1)$th event starts at the instant $t_{0(k+1)} \equiv t_{2(k)}$ which is the end point of kth event. Thus the final values of the variables for the kth event are the initial values for the $(k+1)$th event. The equations representing the two intervals of the $(k+1)$th event can be written in the same way as those of the kth event.

Equations (2, 3), describing the kth event along with those corresponding to the $(k+1)$th event, describe one full cycle of the LCL converter operation. The initial values of the $(k+1)$th event are expressed in terms of the initial values of the kth event.

3.2 The discrete state space model

3.2.1 Selection of discrete state variables

The following discrete state variables were chosen (corresponding to the storage elements in the circuit) for the kth and $(k+1)$th events:

$$x_{1(k)} = -\nu_c^n(t_{0(k)}), \tag{4}$$

$$x_{2(k)} = -i_1^n(t_{0(k)}), \tag{5}$$

$$x_{3(k)} = -i_2^n(t_{0(k)}), \tag{6}$$

$$x_{1(k+1)} = \nu_c^n(t_{0(k+1)}), \tag{7}$$

$$x_{2(k+1)} = i_1^n(t_{0(k+1)}), \tag{8}$$

$$x_{3(k+1)} = i_2^n(t_{0(k+1)}). \tag{9}$$

Concerning the output stage of the LCL converter, we introduce a current source $i_{\text{out}}(k)$ (Fig. 1) which represents the disturbance in the load current. This current value is equal to zero during the steady state [6,7].

The output equation brought back to the primary of the transformer is given by:

$$x_{4(k+1)} = x_{4(k)} + \frac{\gamma_{(k)}}{C_s/C}\left[x_{5(k)} + i_{\text{out}(k)} - \frac{x_{4(k)}}{R_s/Z}\right]$$

where,

$$x_{4(k)} = V_s^n(t_{0(k)}), \tag{10}$$

$$x_{5(k)} = I_s^n(t_{0(k)}), \tag{11}$$

$$x_{4(k+1)} = V_s^n(t_{0(k+1)}), \tag{12}$$

where, I_s^n is the output current.

In order to simplify the presentation of the recurrent equations, L_1 and L_2 are supposed to be equal.

3.2.2 Formulation of the model

Using the states variables defined in the equations (4) to (12) and the equations (2) and (3), the following large signal model, in discrete time domain, is obtained:

$$\begin{aligned}x_{1(k+1)} = &-\cos(\gamma_{(k)})x_{1(k)} - \sin(\gamma_{(k)})[x_{2(k)} - x_{3(k)}] \\ &+ \frac{1}{2} - \frac{x_{4(k)}}{2} - \left[\frac{1}{2} - \frac{x_{4(k)}}{2}\right]\cos(\gamma_{(k)}) \\ &+ x_{4(k)}\cos(\gamma_{(k)} - \alpha_{(k)})\end{aligned} \tag{13}$$

$$\begin{aligned}x_{2(k+1)} = &\frac{\sin(\gamma_{(k)})}{2}x_{1(k)} - \frac{\cos(\gamma_{(k)})}{2}[x_{2(k)} - x_{3(k)}] \\ &+ \left[\frac{1}{4} + \frac{x_{4(k)}}{4}\right]\sin(\gamma_{(k)}) - \frac{x_{4(k)}}{2}\sin(\gamma_{(k)} - \alpha_{(k)}) \\ &- \frac{x_{2(k)}}{2} - \frac{x_{3(k)}}{2} - \frac{\alpha_{(k)}x_{4(k)}}{2} + \frac{\gamma_{(k)}}{4} + \frac{\gamma_{(k)}x_{4(k)}}{4}\end{aligned} \tag{14}$$

$$\begin{aligned}x_{3(k+1)} = &-\frac{\sin(\gamma_{(k)})}{2}x_{1(k)} + \frac{\cos(\gamma_{(k)})}{2}[x_{2(k)} - x_{3(k)}] \\ &- \left[\frac{1}{4} + \frac{x_{4(k)}}{4}\right]\sin(\gamma_{(k)}) + \frac{x_{4(k)}}{2}\sin(\gamma_{(k)} - \alpha_{(k)}) \\ &- \frac{x_{2(k)}}{2} - \frac{x_{3(k)}}{2} - \frac{\alpha_{(k)}x_{4(k)}}{2} + \frac{\gamma_{(k)}}{4} + \frac{\gamma_{(k)}x_{4(k)}}{4}\end{aligned} \tag{15}$$

$$\begin{aligned}x_{4(k+1)} = &x_{4(k)} - \frac{ZC\gamma_{(k)}x_{4(k)}}{R_sC_s} \\ &+ \frac{C}{C_s}\left[\frac{x_{1(k+1)}}{2} + \left(x_{1(k)} + \frac{1}{2} + \frac{x_{4(k)}}{2}\right)\cos(\alpha_{(k)})\right. \\ &-\frac{x_{1(k)}}{2} + (x_{2(k)} - x_{3(k)})\sin(\alpha_{(k)}) - (x_{2(k)} + x_{3(k)}) \\ &\times\left(\alpha_{(k)} + \frac{\gamma_{(k)}}{2}\right) - \alpha_{(k)}^2\frac{x_{4(k)}}{2} - \left(\frac{1}{8} + \frac{x_{4(k)}}{8}\right)\gamma_{(k)}^2 \\ &\left.+\alpha_{(k)}\gamma_{(k)}\frac{x_{4(k)}}{2} + \frac{\alpha_{(k)}^2}{4} - \frac{1}{2} - \frac{x_{4(k)}}{2} + i_{\text{out}(k)}\right].\end{aligned} \tag{16}$$

These non-linear discrete equations have the following general form for $i = 1 \ldots 4$:

$$x_{i(k+1)} = f_i(x_{1(k)}, x_{2(k)}, x_{3(k)}, x_{4(k)}, i_{\text{out}(k)}, \gamma_{(k)}). \tag{17}$$

3.3 Equilibrium point and constant load characteristics

3.3.1 Equilibrium point

Applying the symmetry conditions $x_{i(k+1)} = x_{i(k)}$. The equilibrium point can be determined. The variables $x_{4(k)}$ and $\gamma_{(k)}$ define the equilibrium. Simultaneous solution of the resultant equations yields the following steady-state solution

$$\begin{aligned}x_{1(k)} = &-\left\{[1 + \cos(\gamma_{(k)})]\frac{x_{4(k)}}{\beta} + [\cos(\gamma_{(k)} - \alpha_{(k)})\right. \\ &\left.+\cos(\alpha_{(k)})]\frac{x_{4(k)}}{\beta}\right\}\frac{1}{[1 + \cos(\gamma_{(k)})]}\end{aligned} \tag{18}$$

$$\begin{aligned}x_{2(k)} = &\left\{\frac{\gamma_{(k)}}{2(\lambda + \beta)} + \frac{\gamma_{(k)}\lambda x_{4(k)}}{\beta(\gamma + \beta)} - \frac{\alpha_{(k)}x_{4(k)}}{\lambda + \beta}\right. \\ &+\left[-\frac{\beta}{\lambda}\frac{\sin(\gamma_{(k)})}{\lambda + \beta} + [\sin(\gamma_{(k)} - \alpha_{(k)})\right. \\ &\left.\left.-\sin(\alpha_{(k)})]\frac{x_{4(k)}}{\lambda + \beta}\right]\right\}\frac{1}{1 + \cos(\gamma_{(k)})}\end{aligned} \tag{19}$$

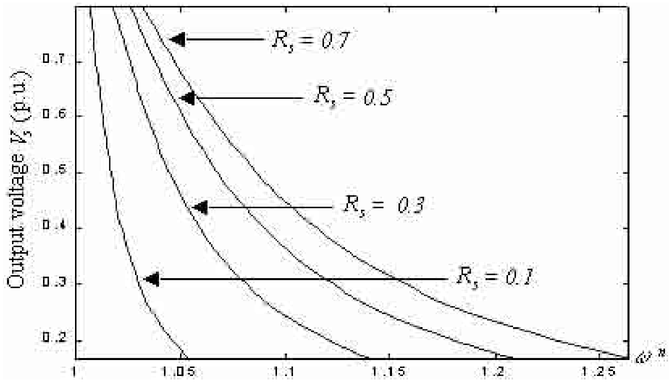

Fig. 4. Constant load characteristics.

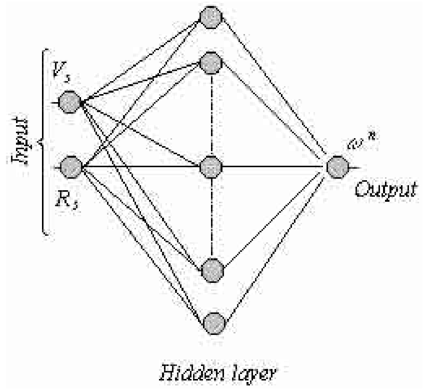

Fig. 5. Neural network structure.

$$x_{2(k)} = \left\{ \frac{\gamma_{(k)}}{2(\lambda+\beta)} + \frac{\gamma_{(k)}\lambda x_{4(k)}}{\beta(\lambda+\beta)} - \frac{\alpha_{(k)}x_{4(k)}}{\lambda+\beta} - \frac{\sin(\gamma_{(k)})}{\lambda+\beta} + [\sin(\gamma_{(k)} - \alpha_{(k)}) - \sin(\alpha_{(k)})] \frac{\lambda}{\beta} \frac{x_{4(k)}}{\lambda+\beta} \right\} \frac{1}{1+\cos(\gamma_{(k)})} \quad (20)$$

where α_k is given by the following equation:

$$\sin\left(\frac{\gamma_{(k)}}{2} - \alpha_{(k)}\right) - x_{4(k)}\sin\left(\frac{\gamma_{(k)}}{2}\right) + \left[\alpha_{(k)} - \frac{\gamma_{(k)}}{2} - x_{4(k)}\frac{\gamma_{(k)}}{2}\right]\cos\left(\frac{\gamma_{(k)}}{2}\right) = 0. \quad (21)$$

3.3.2 Constant load characteristics

In order to have constant load characteristics, the output voltage $V_\mathrm{s} \equiv x_4$ is represented as function of the input frequency. These characteristics are drawn for $R_\mathrm{s} = 0.1, 0.3, 0.5$, and 0.7 (Fig. 4).

4 Artificial neural network

This section presents an overview of the architecture and the learning of the feedforward neural networks used in the control of the LCL converter.

4.1 Neural architectures

The network architecture is defined by the basic processing elements and the way in which they are interconnected. The basic processing element of the connectionist architecture is often called a neurone or unit by analogy with neurophysiology. It is known that the feedforward neural networks (NNs) are capable of implementing any input-output mapping, provided that they have sufficient number of hidden units with non-linear activation functions [8]. The NNs consists of a set of units that constitute the input layer, one or more hidden layers, and an output layer. Both hidden and output layers are made of computation units whereas the input layer is made of non-computation units [9].

In this paper we consider a feedforward neural network with two input units, a single hidden layer, and single output unit as shown in Figure 5. The input layer units are fully connected to the hidden layer units, which are fully connected to the output unit. The output y_i of the ith unit in the hidden layer is given by

$$y_i = f(w_{i1}V_\mathrm{s} + w_{i2}R_\mathrm{s} + \theta_i) \quad (22)$$

where w_{ij} is the synaptic weight on the connection from the jth unit of the input layer to the ith unit of the hidden layer, θ_i is the bias of the ith unit and f is the activation function given by

$$f(x) = \frac{1}{1+\mathrm{e}^{-x}} \cdot \quad (23)$$

The network output is given by

$$\omega^n = \sum_{i=1}^{N} a_i y_i + \theta_s \quad (24)$$

where, a_i is the synaptic weight on the connection from the ith unit of the hidden layer to the output unit and θ_s is the bias of the output unit.

4.2 Learning

The performance of a neural network (NN) depends on a number of parameters, specially the weights. The correct choice of the weights is be done by a learning algorithm.

The back-propagation algorithm (BP) is the most widely applied training algorithm in NNs [10]. The BP is a stochastic gradient descent optimisation procedure minimisation of the mean-squared error (objective function) given bellow

$$E = \frac{1}{2P}\sum_{p=1}^{P}\sum_{k=0}^{K}(\tau_k^p - o_k^p)^2$$

where P is the number of patterns in the training set, K is the number of units in the output layer, and τ_k^p is the

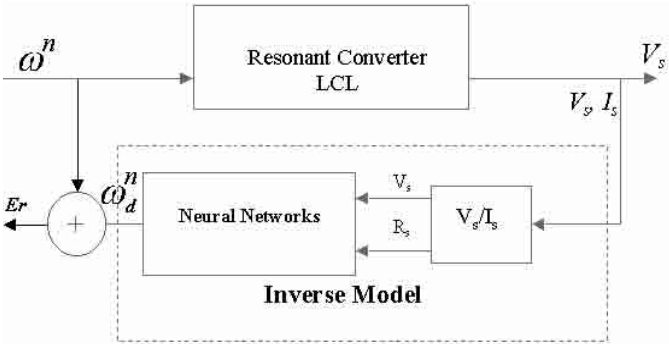

Fig. 6. Structure for inverse neural network modelling.

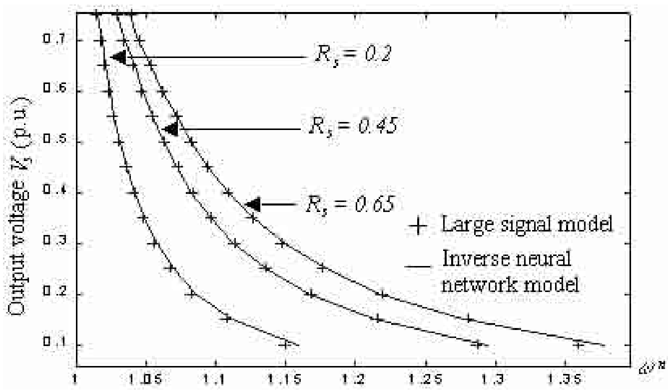

Fig. 7. Constant load characteristics obtained by inverse neural network model, compared with the large signal model.

target output and o_k^p practical output of the kth unit when the pth pattern is presented to the network.

The BP updates the weights after each presentation of a subset of the training patterns (where the subset may range from a single pattern to the whole training set) according to the following equation

$$w_{ij}(t+1) = w_{ij}(t) - \eta \frac{\partial E}{\partial W_{ij}}$$

where η is called learning rate.

5 Control structure

In the particular context of LCL-type resonant converter, the aim of the control scheme is to maintain the output voltage constant in spite of a large change of the load.

The large-signal model of the LCL converter revealed that the converter is strongly a non-linear system, therefore this paper presents a direct inverse control scheme [5] of the LCL converter based on a neural network that is also a non-linear system.

The direct inverse control scheme relies heavily on the fidelity of the inverse model (*i.e.* the trained neural network). To obtain an inverse neural model of the LCL resonant converter, the network is trained using the output voltage of the converter and the load as an input vector, and the converter input frequency as the target output. The obtained inverse system is then cascaded with the LCL converter such that the composed system results in an identity mapping between desired response and the LCL output voltage. Thus the network acts directly as a controller.

To obtain the inverse model of Figure 6, the network is trained by the back-propagation learning algorithm using the 336 equilibrium points data used to plot the characteristics in Figure 4. Each equilibrium point is given by V_s, ω^n and R_s.

At each iteration of the learning, a voltage V_s and a load R_s are presented at the networks input, and the weights are updated such that the difference between the practical network output and the desired output frequency is minimised.

After the convergence of the learning process, the network is tested on 336 other equilibrium points (R_s = 0.2, 0.45, 0.65, 0.8). The results presented in Figure 7, show that the network matches the inverse system accurately.

The trained network (*i.e.* the inverse system of the converter) is then cascaded with the LCL converter (Fig. 8).

The desired output voltage of the converter is presented at the neural network's input, then the network calculates the necessary control frequency of the converter. In the case of a large variation of the load, the network supplies the necessary frequency to the converter such that the output voltage is maintained constant despite of large changes of the load.

6 Simulation results

6.1 Converter specifications

The LCL-type resonant converter designed has the following specifications:
Input supply voltage $V_e = 150$ V.
Output voltage of the converter $V_s = 82$ V.
Maximum output power $P = 150$ W.
Switching frequency, $f_0 = 150$ kHz.
The design values obtained are:
$L_1 = L_2 = 192$ μH; $C = 13.3$ nF; $C_s = 10$ mF.
The total converter is simulated using Simulink software.
MOSFET model is used to simulate the active switch.

6.2 Results

The load is passed from $R_{s_1} = 41.35$ Ω (the equilibrium point is defined by: $V_{s_1} = 0.525$, $\omega_1^n = 1.065$ and $R_{s_1} = 0.5192$) to the value $R_{s_2} = 0.2837$ which is equivalent to 54.64% change in the load. Without any control strategy, this variation of the load causes a change in the output voltage which passes from $V_{s_1} = 0.525$ to $V_{s_2} = 0.3550$. Using the proposed control scheme, the neural network calculates the control frequency which permits to maintain the output voltage constant $V_{s_1} = 0.525$. The adequate control frequency is equal to $\omega_2^n = 1.04$.

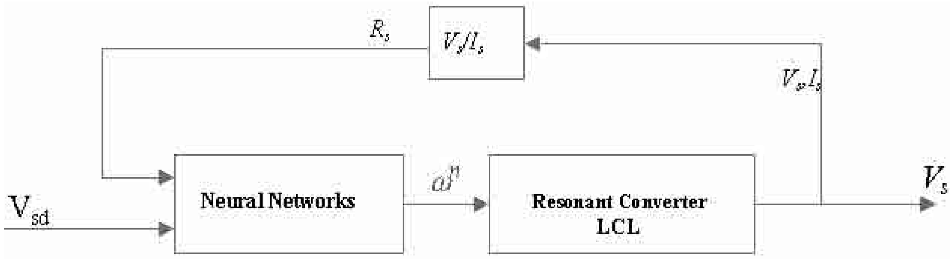

Fig. 8. Structure for neural control of the LCL resonant converter. ω^n: operating frequency, V_{sd}: desired output voltage, V_s: output response, R_s: load.

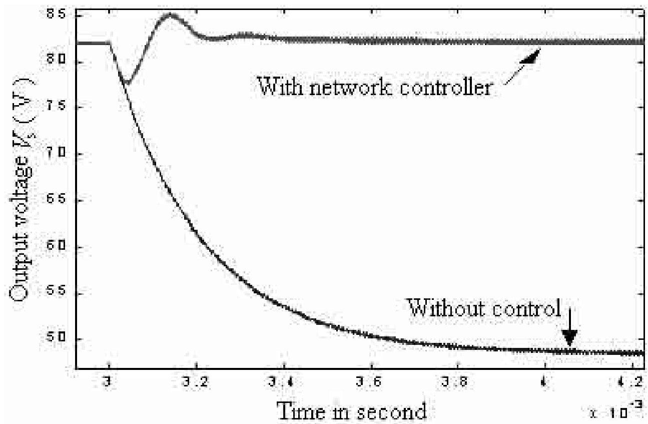

Fig. 9. The output voltage in the case of a large variation of the load (Simulink results).

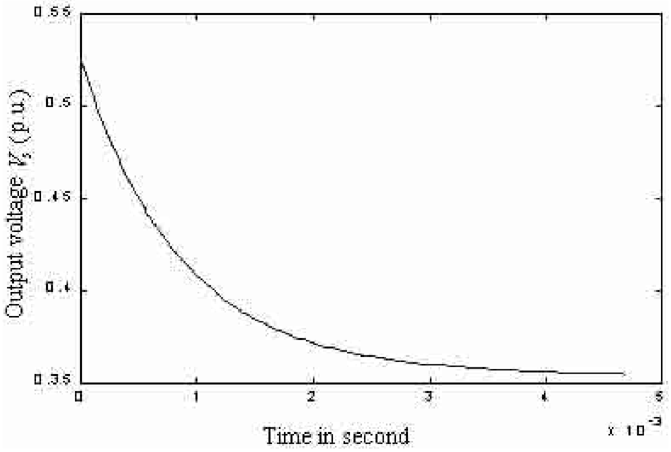

Fig. 10. Output response of the LCL converter without any controller.

Figure 9 illustrates the efficiency of using the proposed control scheme.

6.3 Transient analysis

The dynamic analysis is useful for better understanding and designing the converter. A discrete time model for the LCL converter is derived. The large signal analysis determines the response of the converter when its operating conditions undergo large variations in their steady-state values and is therefore useful for choosing appropriate component ratings.

The dynamic response of the converter during the transient events is bound to govern proper design procedure and the choice of an appropriate control scheme. Using the large signal model, based on discrete time domain, we analyse the output's response when the above neural network controls the LCL converter.

Without using any controller, the converter output voltage changes depending on the load. A large variation of the load results in a significant variation of the output voltage (Fig. 10). Using the large signal model, we analysed the transient behaviour of the converter in the case of a large variation of the load. The simulation results show the efficiency of using the neural network controller. In fact, when the load changes, the output voltage oscillates for a short time then stabilises at the desired output voltage (Fig. 11). The results show that the neural network is a good regulator of the LCL converter.

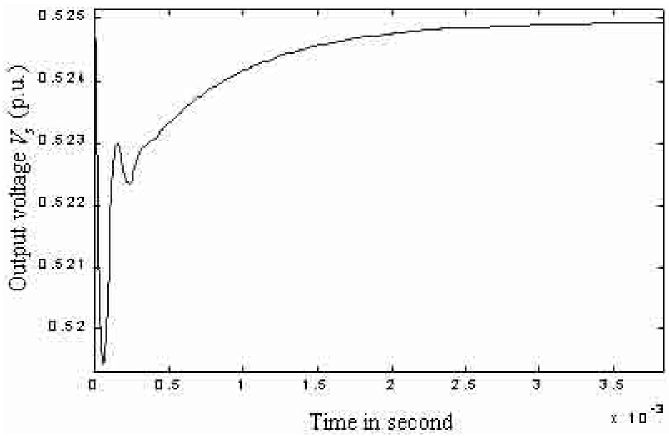

Fig. 11. Output response of LCL converter using neural network controller.

7 Conclusion

In this paper a discrete time domain model has been derived for the LCL converter for continuous conduction and lagging power operation modes. Using this model, a few calculations are sufficient to predict the transient behaviour of the converter from a designer's point of view.

In order to maintain the output voltage constant in spite of a large change of the load, a neural network inverse model is designed. To obtain an inverse neural model of the LCL resonant converter, the network is trained using the output voltage of the converter and the load as an input vector, and the converter input frequency as the target output. The obtained inverse system is then cascaded with the LCL converter such that the composed system results in an identity mapping between desired response and the LCL output voltage. Thus the network acts directly as a controller.

The large signal model, based on discrete time domain, is used to predict the behaviour of the converter at the time of the change of the load. The simulation results show the efficiency of using neural networks to regulate the LCL converter. These results are also verified using Simulink software.

The prospective of this work is to improve the output voltage response in dynamic and steady state operation of the LCL converter. Moreover we intend to use the neural control when the converter operates in the pulse wide modulation PWM mode.

References

1. Kh. Louati, D. Sadarnac, *Analysis of resonant Converter with LCL-type Commutation, EPE'93*, pp. 141-147.
2. Kh. Louati, W. Abida, D. Sadarnac, *Analysis of the LCL-Resonant Converter Operating Above Resonance, EPE'95*, pp. 2.839-2.844.
3. H. Azzam, G. Bornard, S. Bacha, M. Brunello, *Definition and Application of a non-linear control law for series resonant converters, PESC'92*, pp. 793-799.
4. S. Zouggaar, H. Nait Charif, G. Rojar, M. Azizi, *Dynamic Analysis and Control Design of the LCL-Type Resonant Converter, EPE'99*, 7-9 September 1999.
5. K.J. Hunt *et al.*, Neural networks for control system - a survey, *Automatica* (Pergamon Press Ltd, 1992), pp. 1083-1112.
6. R.P. Lippmam, *An Introduction to Computing with Neural Net*, IEEE ASSP Magazine, April 1987, pp. 4-22.
7. V. Agrawal, A.K.S. Bhat, IEEE Trans. Power Electron. **10**, 222 (1995).
8. K. Funabashi, On the approximate realization of continuous mappings by neural networks, *Neural Networks* (Pergamon Press Ltd, Oxford, England, 1989), Vol. 2, pp. 183-192.
9. N.C. Hammadi, H. Ito, IEICE Trans. Information & Systems **E80-D**, 21 (1997).
10. N.C. Hammadi, Design of Fault Tolerant Feedforward Neural Networks, Ph.D. thesis, Graduate School of Science and Technology Chiba University, March 1998.

to access this journal online:
www.edpsciences.org